

Microstructure and Mechanical Properties of Friction Stir Welded Al–Mg–Si Alloys Under Variable Parameter Conditions

Manu Srivastava¹ · Nasir Khan² · Shazman Nabi³ · Sandeep Rathee³ 

Received: 9 May 2023 / Accepted: 23 June 2023 / Published online: 8 August 2023
© The Institution of Engineers (India) 2023

Abstract The current study investigates the variation of mechanical properties and microstructural evolution with varying process parameters for Al–Mg–Si (AA6061-T6) alloys during friction stir welding (FSW) process. The experiments were designed using Taguchi’s technique, with three tool factors being examined—rotational speed (RST), traverse speed (TST), and shoulder diameter (SDT)—at three different levels each. L27 Orthogonal array has been utilized to analyze the effect of these parameters upon mechanical strength. Experimental results were analyzed both quantitatively and qualitatively, with statistical techniques being used for quantitative analysis, and microstructural evolution being used for qualitative analysis. The study found that traverse speed of tool had the most significant effect on ultimate tensile strength, with a contribution of 25.94%, followed by shoulder diameter of tool (25.86%) and rotational speed of tool (20.30%). Furthermore, the study found that the interactions between selected parameters had a significant impact on mechanical strength. Interaction between TST and SDT contributed 14.10%, that between RST*TST contributed 6.51% and the least contribution is between RST and SDT which is around 3.10%. Results of mechanical strength were found to agree with observations related to microstructural analysis for the FSW joints.

Keywords Friction stir welding · Tensile strength · Microstructural evolution · Optimization · Taguchi technique · Al–Mg–Si alloys

Introduction

Friction stir welding (FSW) offers an impressive spectrum of benefits in achieving sound-quality welds of lightweight materials. It can be considered one of the most significant developments in solid-state joining techniques. FSW is a green technology as it works below the melting point temperature of base metal (BM) and welds formation occurs in solid state [1–4]. Joining is accomplished by inserting a rotating non-consumable tool into the line of abutting edges of BM plates (clamped in the fixture) followed by tool traverse. Heat generation takes place owing to frictional heat and severe plastic deformation.

FSW is widely used in several applications, such as in aerospace, automotive, and marine, and is attracting research since its invention in 1991 [5]. Different FSW derivatives including but not limited to friction stir processing [6–10], friction stir channeling [11], and some advanced processes like friction-based additive manufacturing are getting popularity [12–15]. Regarding the FSW of similar alloys, several researchers work on Al 2xxx, 5xxx, 6xxx and 7xxx series alloys [16–21]. Both microstructural and mechanical characteristics were reported to vary with welding speed for AA6061-T6 aluminum alloy as reported by Liu et al. [22]. The plate thickness utilized was 4 mm, with RST of 600 rpm. 50–200 mm/min welding speed window was considered. The major observation of this study was increasing tensile strength corresponding to increased welding speed. FSW of AA6061 alloy was investigated by Malopheyev et al. [23], examining welding speeds of 125, 380, and 760 mm/

✉ Sandeep Rathee
rathee8@gmail.com

¹ Department of Mechanical Engineering, PDPM Indian Institute of Information Technology, Design and Manufacturing, Jabalpur, India

² Department of Mechanical Engineering, Amity University Madhya Pradesh, Gwalior, India

³ Department of Mechanical Engineering, National Institute of Technology Srinagar, Jammu and Kashmir, India

Table 1 Chemical composition of AA6061-T6 alloy (wt%)

Element	Mg	Si	Cu	Zn	Ti	Mn	Cr	Al
Amount (wt%)	0.85	0.68	0.22	0.07	0.05	0.032	0.06	Balance

min. The study examined the impact of different welding speeds on both microstructural and mechanical characteristics, finding that an increase in welding speed prevented precipitation coarsening, resulting in an increase in weld strength. These findings highlight the significant impact that welding speed can have on both microstructural as well as mechanical properties of FSWed aluminum alloys.

To summarize, several research on FSW of AA 6061 alloys have been published thus far, looking at the effects of both the individual and combined process factors. There are not many recorded works on thick sheets of AA6061 metal, though. Up to best of authors' information, there is hardly any reported research related to impact of interactions between process parameters for AA6061-T6 aluminum alloys. Mechanical strength of FSWed joints is estimated in this study based upon parametric influence of selected process variables. Also, effect of interactions between process parameters is evaluated.

Experimental Procedure

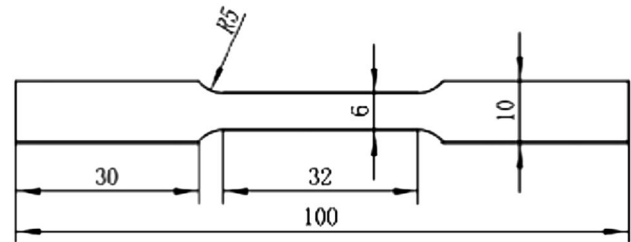
AA6061-T6 alloy base metal (BM) in the form of plates is utilized for the present experimentation. Details of BM composition are presented in Table 1. Initially, BM was processed via CNC vertical milling machine to obtain a uniform size of 150 mm length, 80 mm width and 8 mm thickness. These plates were cleaned using acetone in order to remove dust, grease, etc. These plates were firmly clamped on an in-house developed fixture in butt weld position. Then, FSW has been carried out using a vertical milling machine that has been suitably modified and retrofitted. The experimental procedure involved a series of trial experiments to determine both the variable and fixed process parameters. The initial experiments were conducted to identify the optimal fixed parameters and their values. After these were determined, additional trial experimentations were carried out for establishing a process parameter working window. For the variables (TST, RST and SDT), a process window was developed based on the fact that all trials carried out in the established range produced sound welds. Constant FSW parameters are presented in Table 2 and range/levels of the variable parameters is given in Table 3, respectively. This process of trial experimentation and window determination

Table 2 Constant process parameters

Process parameters	Value taken
Tool pin profile	Cylindrical threaded
Tool shoulder profile	Flat
Tool pin diameter	8 mm
Tool pin length	7.8 mm
Tilt angle	2°
Tool plunge depth	0.25 mm

Table 3 Working range of variable parameters

Symbol	Input parameters	Range of parameters	Levels		
			(1)	(2)	(3)
A	RST (rpm)	700–1120	700	900	1200
B	TST (mm/min)	40–80	40	60	80
C	SD (mm)	20–24	20	22	24

**Fig. 1** Dimensions of tensile specimen

is a common approach in materials processing research, as it allows for the identification of optimal process parameters that can maximize product quality while minimizing defects and waste.

To facilitate the experimental work depending on the number of parameters used and their respective levels, L27 orthogonal array (OA) of Taguchi was employed. After completion of all FSW passes (single pass), samples for microstructural analysis were prepared from welded zone using wire electric discharge machining (EDM). These samples were polished using different grades of emery papers followed by cloth polishing using alumina and then etched for 30 s with Keller's reagent. Then, these

samples were analyzed using optical microscope. Tensile samples were prepared according to ASTM standards (as shown in Fig. 1) machined in traverse direction to FSW route using wire EDM. To ensure accuracy and facilitate statistical analysis, tensile testing was conducted using a computerized tensiometer. Each run was replicated thrice, and average result of the three values was calculated and

analyzed to obtain meaningful conclusions. This approach ensured that the experimental results were reliable and reproducible.

Results and Discussion

Tensile Strength

Table 4 presents ultimate tensile strength (UTS) values determined for the welded samples using Minitab 17 software [24]. Because greater UTS values are preferable, the findings were evaluated using a higher-the-better quality characteristic. For identification of ideal process parameter combination for obtaining the maximum tensile strength of the fabricated joints, the *S/N* or signal-to-noise ratio is considered.

Based on the rank of the process variables for FSW (refer Table 5), it can be concluded that traverse speed of tool (TST) has the most significant effect on UTS, followed by the shoulder diameter of tool (SDT) and rotational speed of tool (RST). Figure 2 depicts the means main effect plots for UTS. Upon careful analysis of responses for *S/N* ratio and means of UTS, depicted in Table 5 and Fig. 2, it can be concluded that optimal combination of process parameters to achieve optimal UTS through FSW is A1B3C1 which implies level 1, 3, 1 of RST, TST and SDT, respectively.

ANOVA Results and Regression analysis for UTS

The percentage contribution for chosen process variables for was estimated using ANOVA, and the findings are shown in Table 6.

Effect of Tool Rotation Speed upon UTS

Figure 2 depicts *S/N* ratio for UTS graphically. The plot indicates that increasing RST from level 1 2 amounts to a drop in UTS for welded joints, and that increasing RST further lowers UTS. The drop in UTS from level 2 to 3 is greater as compared to the drop in case of level 1–2. Increased heat generation caused UTS drop owing to increasing RST, which has a substantial impact on the UTS. Heat generation may be

Table 4 Measured values of UTS and percentage elongation

S. No	RST (A)	TST (B)	SDT(C)	UTS (MPa)	Percentage elongation
1	1	1	1	224.222	8.58
2	1	2	2	223.278	8.80
3	1	3	3	216.039	8.55
4	2	1	1	218.647	8.72
5	2	2	2	229.463	8.72
6	2	3	3	222.397	8.66
7	3	1	1	208.747	8.24
8	3	2	2	222.175	8.52
9	3	3	3	215.800	8.26
10	1	1	2	221.432	8.53
11	1	2	3	217.372	8.66
12	1	3	1	238.100	8.62
13	2	1	2	215.457	8.56
14	2	2	3	215.800	8.49
15	2	3	1	238.050	8.59
16	3	1	2	213.500	8.14
17	3	2	3	210.900	8.45
18	3	3	1	224.400	8.46
19	1	1	3	220.900	8.60
20	1	2	1	224.000	8.81
21	1	3	2	225.619	8.60
22	2	1	3	214.022	8.69
23	2	2	1	224.596	8.82
24	2	3	2	223.959	8.62
25	3	1	3	210.105	8.14
26	3	2	1	219.307	8.62
27	3	3	2	221.997	8.42

Table 5 Illustrates the *S/N* ratio of UTS

FSW parameters	Unit	Symbol	Levels			Delta	Rank
			1	2	3		
RST	Rpm	A	46.97	46.94	46.70	0.27	3
TST	mm/min	B	46.70	46.88	47.03	0.33	1
SDT	Mm	C	47.00	46.92	46.68	0.32	2

Fig. 2 Main effect plot of *S/N* ratios for UTS

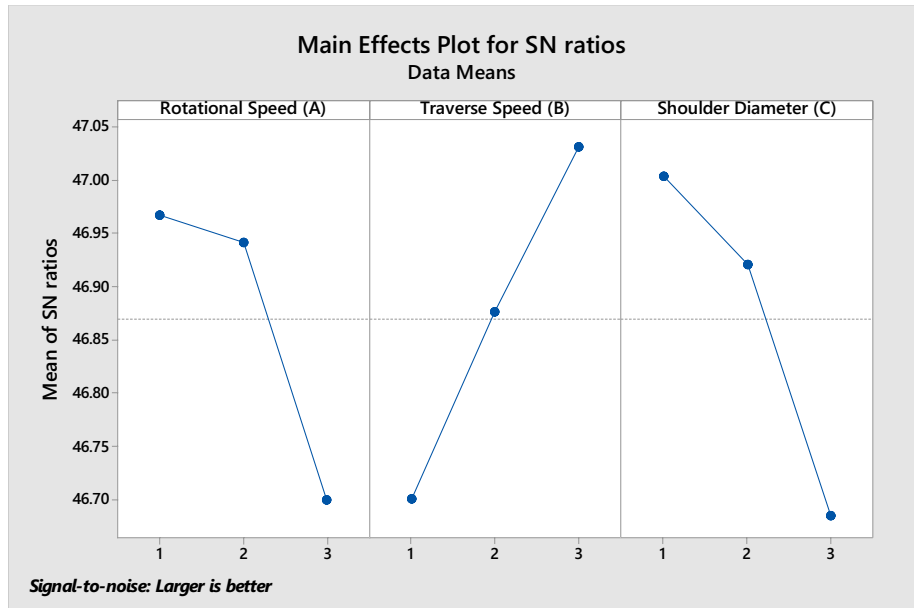


Table 6 ANOVA results and percentage contribution of FSW parameters for UTS

Source	DF	Adj SS	Adj MS	F Value	P Value	Contribution (%)
RST (A)	2	252.34	126.17	19.35	0.001	20.30
TST (B)	2	322.63	161.313	24.74	0	25.94
SDT (C)	2	321.6	160.802	24.66	0	25.86
RST (A)*TST (B)	4	81.05	20.264	3.11	0.05	6.51
RST(A)*SDT (C)	4	38.29	9.572	1.47	0.048	3.10
TST (B)*SDT (C)	4	175.37	43.843	6.72	0.011	14.10
Error	8	52.16	6.52			4.19
Total	28	1243.45				100.0

RST*TST means the combined interaction effect of the rotational speed of the tool (RST), and the shoulder diameter of the tool (SDT). “*” is used for interaction effect

Table 7 Illustrates the *S/N* ratio of percentage elongation

FSW parameters	Unit	Symbol	Levels			Delta	Rank
			1	2	3		
RST	Rpm	A	18.73	18.55	18.69	0.29	1
TST	mm/min	B	18.74	18.74	18.63	0.19	2
SDT	Mm	C	18.44	18.62	18.59	0.10	3

adequate at RST level 1, and when generated heat increases, precipitates dissolve (for heat-treatable Al alloy) and grains enlargement occurs, further lowering UTS.

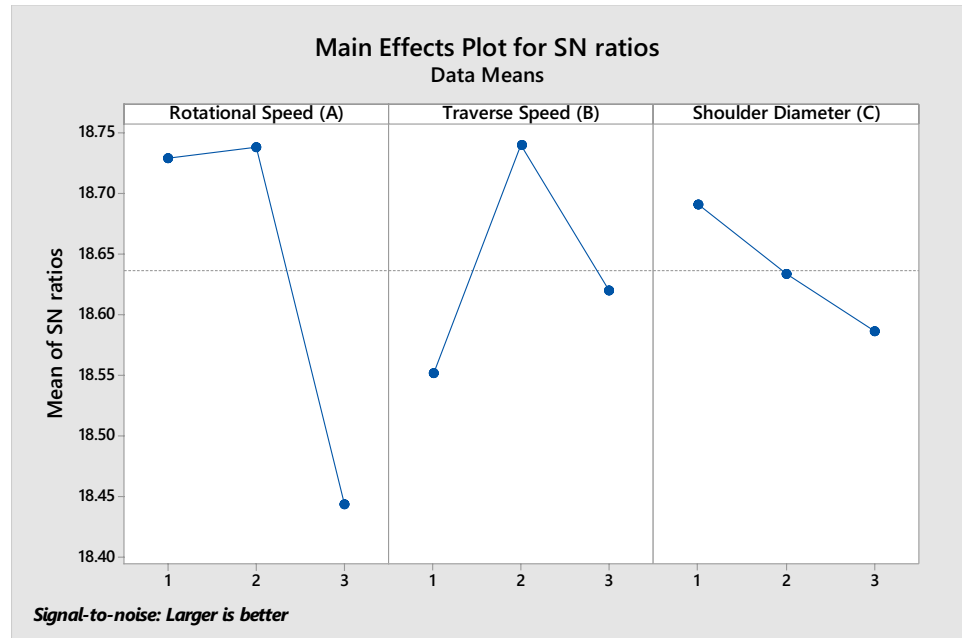
Increasing the RST involves contrary factors that govern UTS. These factors chiefly comprise of material flow as well as softening effect when increased amount of heat is generated. When RST increases, tool stirring effect is increased, improving mixing of material as well as its flow, thereby amounting to enhancement in UTS values. However, with

an increasing RST, the softening effect also increases, that lowers UTS. Effect of material flow is dominated by softening effect thereby lowering the UTS here.

Effect of Tool Traverse Speed upon UTS

Variation of UTS with TST is illustrated in Fig. 2 which indicates that an increasing TST from level 1 to 2 and then 3, leads to an increase in UTS. The reason behind this is that

Fig. 3 Main effect plot of *S/N* ratio for percentage elongation



TST plays a crucial role in dissipating the heat generated during the welding process. This means that with a higher TST, the heat generated during welding is spread over a shorter time interval, resulting in a lower overall heat input. As a result, the chances of grain growth are reduced, leading to a higher UTS. However, when the TST is too high, it may result in poor material mixing due to the decreased total heat input and high tool traverse rate that may decrease UTS. However, in present experimentations, sufficient heat was generated amounting to adequate material mixing. Therefore, UTS increased from level 1 to 2 and then 3 of TST.

Effect of Shoulder Diameter of Tool on UTS

The graph in Fig. 2 represents SDT effect on UTS of FSWed joints. As shown in the graph, the UTS decreases with increasing SDT from level 1 to 2, and further lowers with increasing SDT from level 2 to 3. SDT is an essential parameter in the FSW process as it plays a key role in generating heat and forging the underlying material [3, 7]. As SDT is increased while maintaining constancy of remaining variables, it amounts to an increased heat

input, forging action, and material volume requiring stirring, thereby enhancing UTS.

However, beyond a certain limit, an increase in heat input might cause precipitate dissolution and grain expansion, resulting in reduced weld joint strength. As SDT is increased further, the increasing heat input generates a softening effect which mostly outweighs prior occurrences. As a result, greater UTS may be attained at SDT of level 1 when significant heat is created, sufficient to plasticize, mix, and consolidate material. In summary, the optimal value of SDT can be determined by finding the balance between heat input and softening effect to obtain the highest UTS.

Percentage Elongation

The measurement of percentage elongation was conducted by recording the values before and after the breaking of the tensile specimen, and these values are reported in Table 4. The base metal (BM) showed a percentage elongation of 17%. However, Table 4 indicates that some experiments displayed good percentage elongation, while others showed

Table 8 ANOVA results and percentage contribution of FSW parameters for percentage elongation

Source	DF	Adj SS	Adj MS	F Value	P Value	Contribution (%)
RST (A)	2	0.478252	0.239126	66.61	0	55.41
TST (B)	2	0.155696	0.077848	21.69	0.001	18.04
SDT (C)	2	0.047207	0.023604	6.58	0.02	5.47
RST (A)*TST (B)	4	0.102504	0.025626	7.14	0.009	11.88
RST(A)*SDT (C)	4	0.007726	0.001932	0.54	0.049	0.90
TST (B)*SDT (C)	4	0.043081	0.01077	3	0.05	4.99
Error	8	0.028719				3.33
Total	26	0.863185				100.00

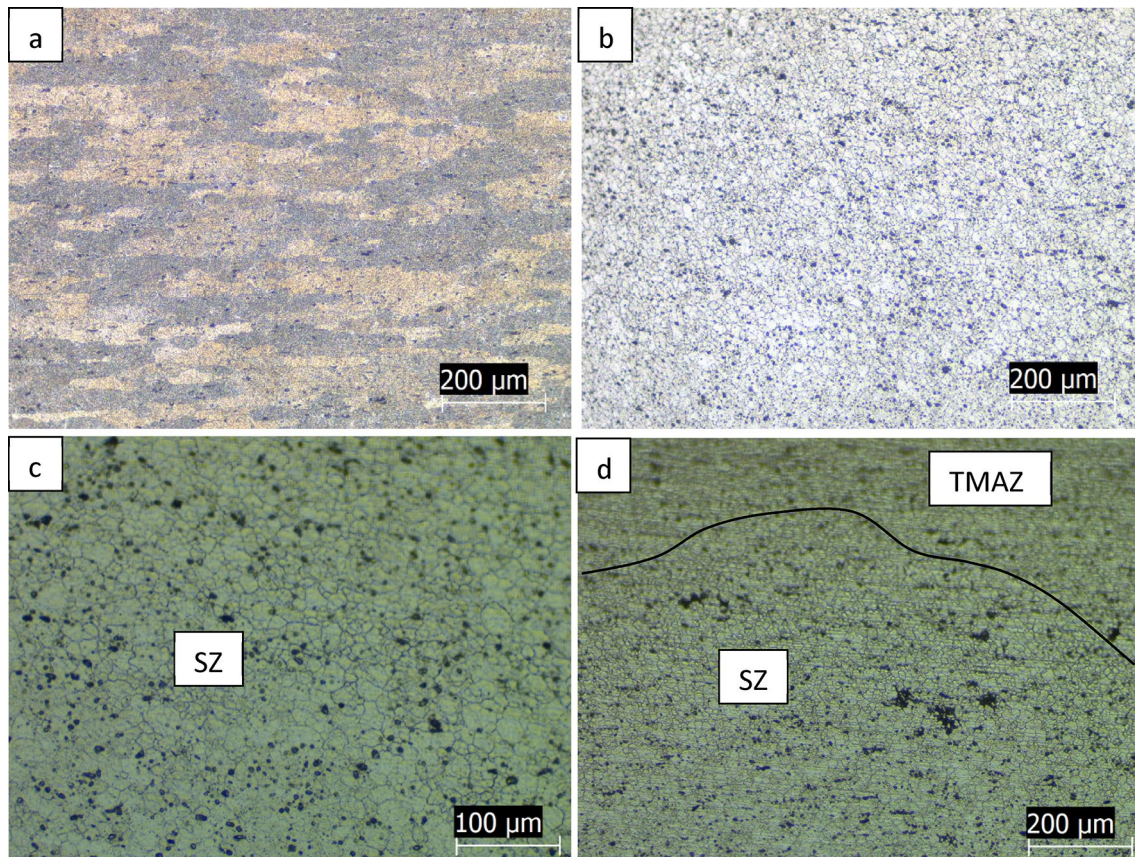


Fig. 4 Microstructural images of: **a** BM; **b**, **c** and **d** sample number 12 at different magnifications

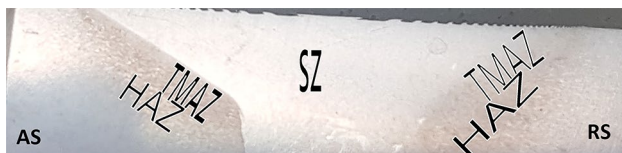


Fig. 5 Macrographic image of sample number 12, illustrating different zones of weld region

low values. The maximum percentage elongation of 8.82% was achieved during the experimentation that is considerably lower than base metal. This is primarily because of increase in tensile strength resulting from severe plastic deformation with recrystallization occurring at the stir and thermo-mechanically affected zones (SZ & TMAZ, respectively) of FSWed joint, leading to reduced ductility. Inter-metallic compound formation has the primary responsibility for the decrease in ductility. *S/N* analysis study, as presented in Table 7, was performed for determining optimal process parameter combination to produce most preferable percentage elongation of the manufactured joints.

RST has the highest influence on percentage elongation, followed by the TST and the SDT, according to the ordering of the FSW process factors. Plotting of *S/N* ratio major effect plots was accomplished which is presented in Fig. 3. Based on *S/N* ratio and main effect plot responses for percentage elongation (Table 7 and Fig. 3, respectively), one can easily infer that optimal percentage elongation was achieved at RST, TST and SDT levels of 2, 2 and 1, respectively, denoted as A2B2C1.

Results of ANOVA and Regression analysis (% elongation)

The percentage contribution of the FSW process parameters was estimated using ANOVA, and the findings are shown in Table 8.

Influence of Tool Rotation Speed on Percentage Elongation

Main effects plot of the *S/N* ratio corresponding to percentage elongation is presented in Fig. 3. The plot reveals that there is a slight increase in the percentage elongation from level 1 to 2, superseded by decreasing value from level 2 to 3. However, the slope of the decrease is steeper than the

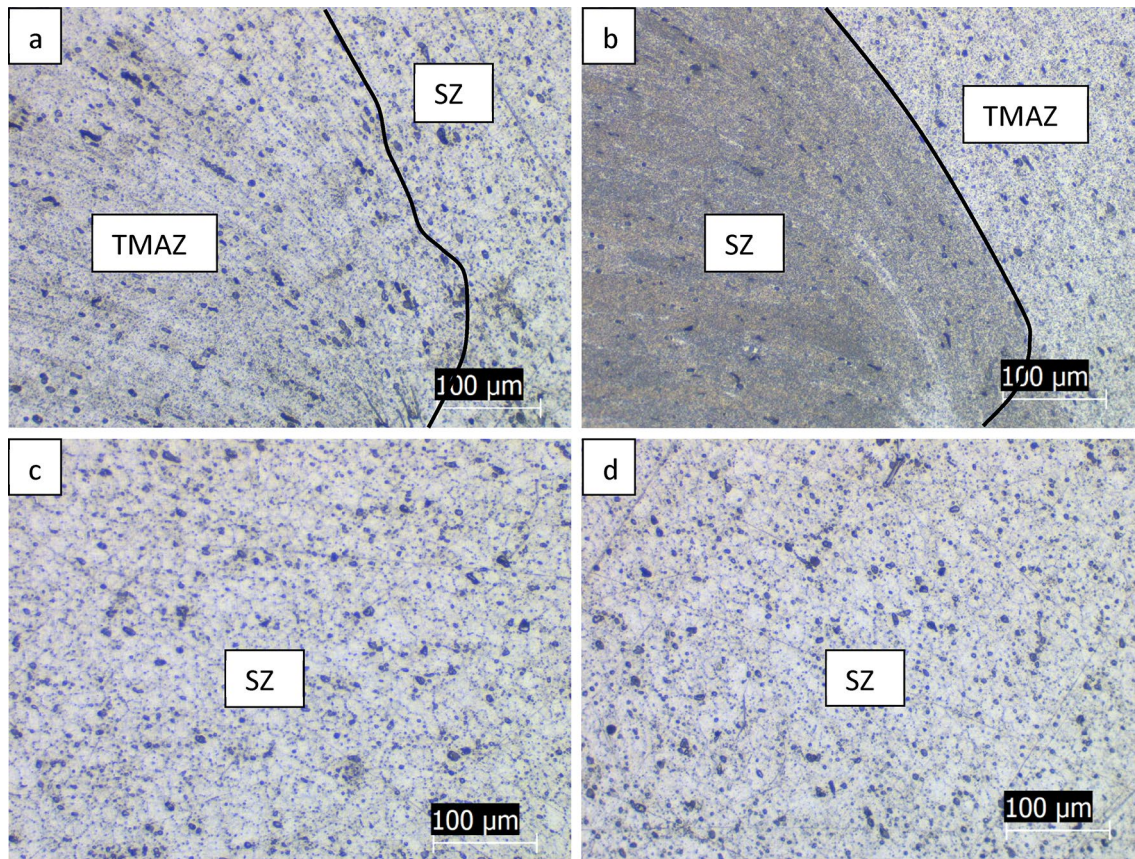


Fig. 6 Microstructural images of: **a** run no. 07; **b** run no. 15; **c** run no. 21; **d** run no. 21

slope for increase. This can be understood as follows: with an increase in RST, there is an improvement in flow and mixing of the material that enhances percentage elongation. However, between level 2 to 3 of RST, excessive heat generation takes place, leading to precipitate dissolution which ultimately tantamount to reduced percentage elongation.

Influence of Traverse Speed of Tool on Percentage Elongation

Main effect plots for *S/N* ratio of % elongation is presented in Fig. 3. It can be observed that there is an increase in percentage elongation initially when TST increases from level 1 to 1 2, followed by decrease as the TST increases from level 2 to 3. This can be understood as follows: with increasing TST, the heat generated by the welding process is dispersed over a shorter interval of time, resulting in a decrease in heat input. This reduces the chances of grain growth and dissolution of precipitates, which can enhance the percentage elongation.

However, as the TST increases further from level 2 to 3, the reduction in heat input can lead to poor material mixing and flow, which can result in lower percentage elongation.

Effect of Shoulder Diameter of Tool on Percentage Elongation

Figure 3 depicts the signal-to-noise ratio (*S/N*) corresponding to % elongation for different SDT levels during FSW. The plot reveals that there is a decreasing trend in the percentage elongation as the SDT level increases from level 1 to level 3. It can be understood as: there is an increase in heat generation and the volume of material stirred with increase in SDT. The % elongation is maximum at an optimal heat generation level. However, if the heat generation level surpasses the adequate amount, it may result in a decrease in % elongation. To conclude, best combination of process parameters to obtain the optimal % elongation is, RST, TST and SDT at levels 2, 2, and 1, respectively, i.e., A2B2C1.

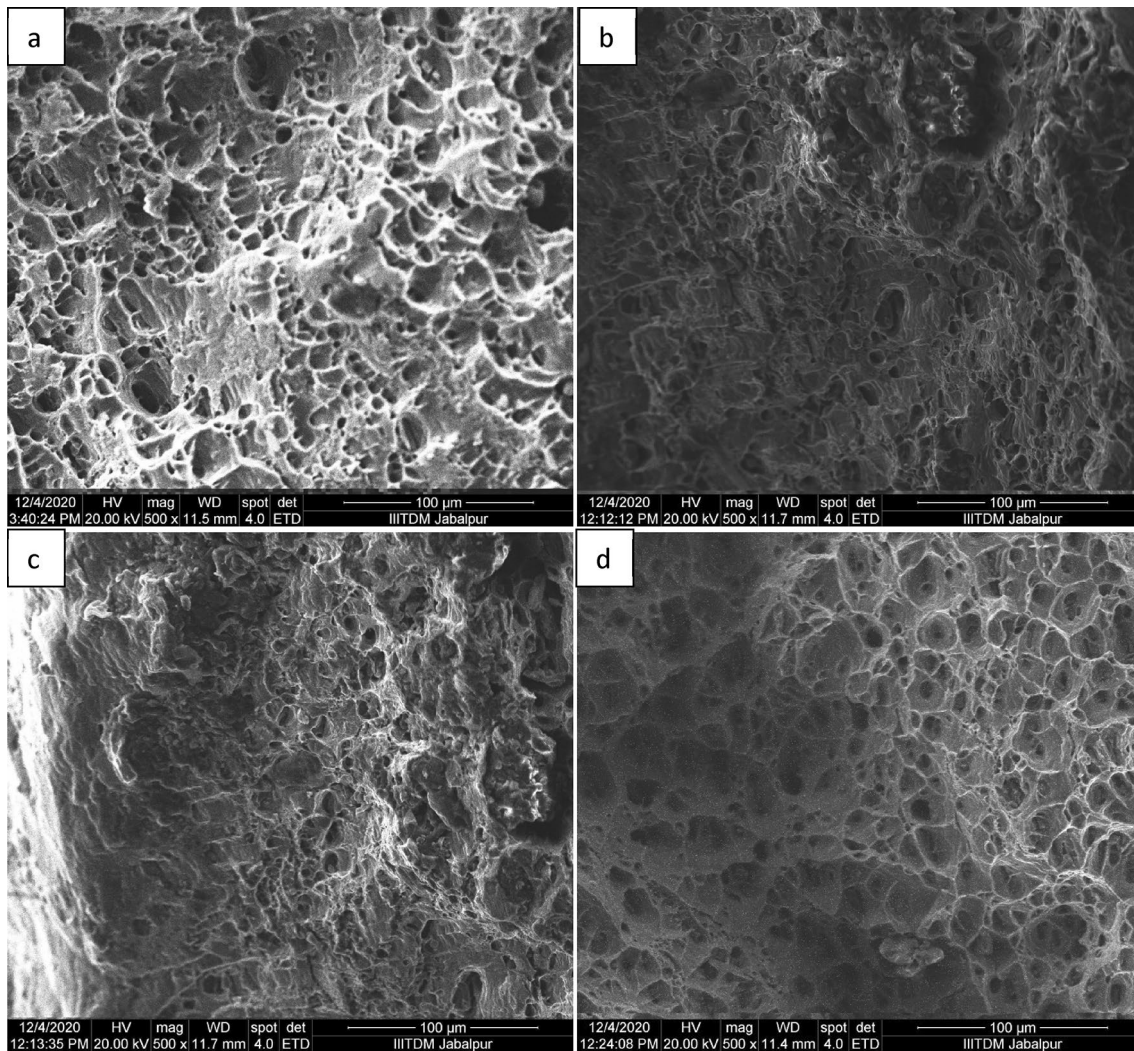


Fig. 7 Fractography images of: **a** run no. 07; **b** run no. 17; **c** run no. 25; and **d** run no. 13

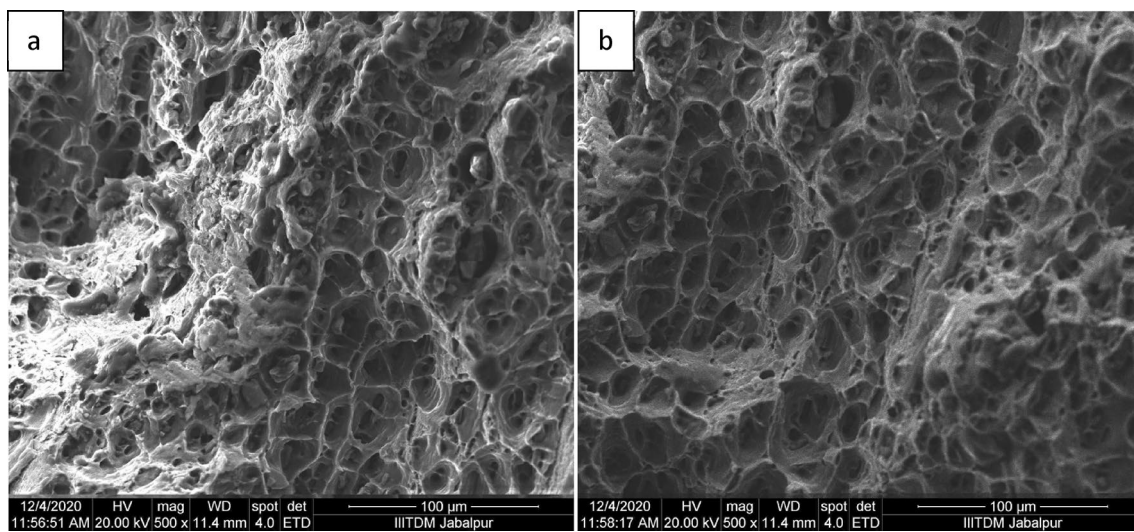


Fig. 8 Fractography images of: **a** run no. 23; and **b** run no. 24

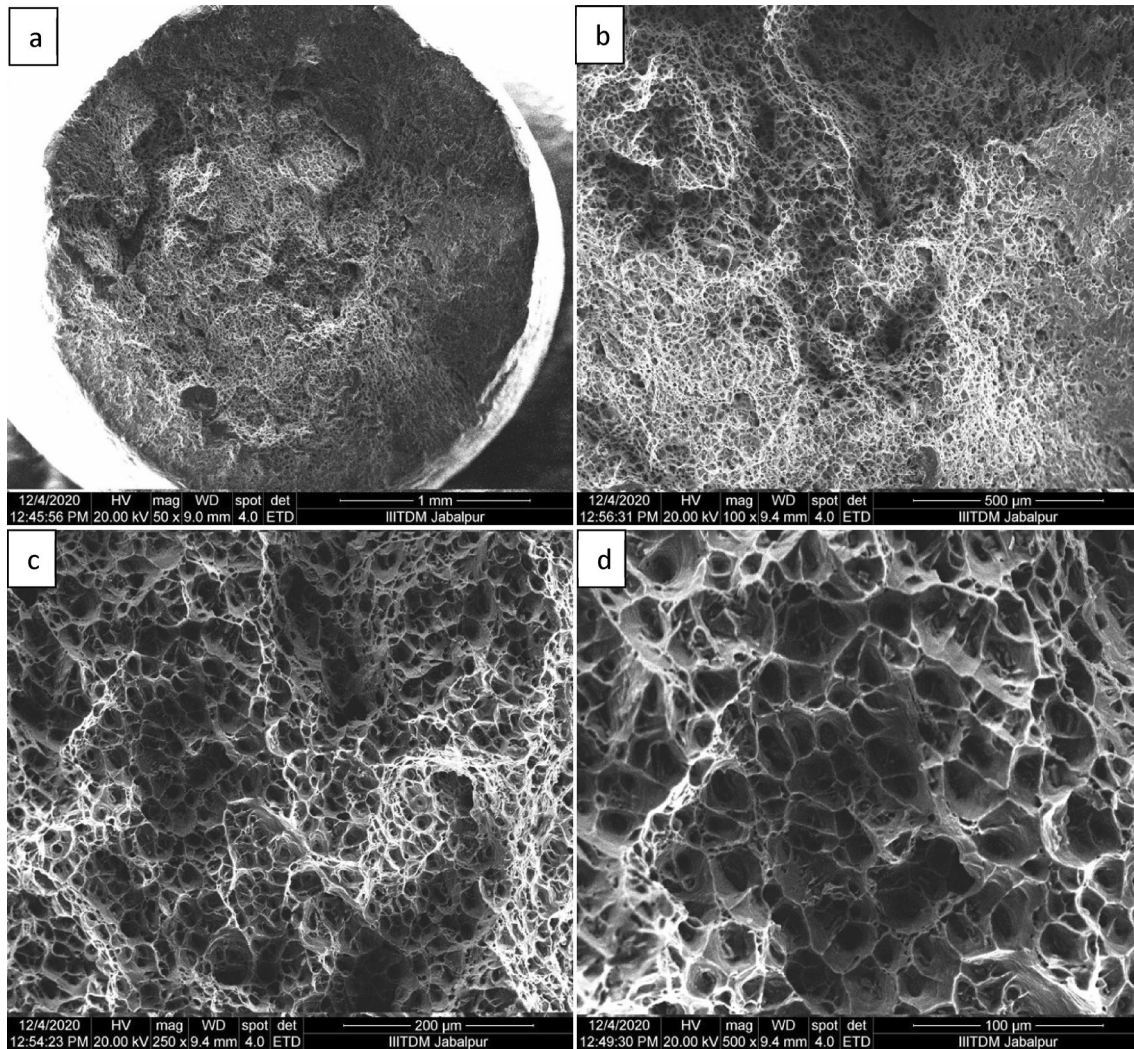


Fig. 9 (a-d) Fractography image of sample number 12 (AS) at different magnifications results

Analyzing the Microstructural Evolution

The optical microscope (OM) was used to capture microstructural images after etching of samples that were obtained from the traverse weld sections. Images were obtained at various orientations and zones like advancing side (AS), retreating side (RS), and stir zone (SZ). A comparison of captured microstructural images with BM of AA6061 alloy was then accomplished. Images of BM microstructure presented as Fig. 4a depicts elongated grains. Microstructure of stir zone for run 12 resulting in highest UTS, are presented by Fig. 4b, c. Different magnification ratios were used to obtain these images. In Fig. 4c, random precipitation, visible as black particles, with fine grains can be seen. Figure 4d shows SZ and TMAZ zones of RS for run 12.

Macrographs for run 12 are presented as Fig. 5, which shows the various FSW zones like stir, thermo-mechanical

affected, heat affected and base metal. Figure 6 shows microstructural images of different experiments. Overall, these images will help the reader in comprehending the microstructural evolution during FSW and can be used to optimize the process parameters to obtain the desired microstructure and properties.

Fractography

In order to understand the cause of joint failure, fractography analysis was carried out on broken tensile specimens. Fractography images of failed specimens are shown in Figs. 7 and 8, displaying different types of dimple characteristics. Some welds show shallow and sparsely populated dimples indicating brittle failure and lower UTS values, as shown in Fig. 7. Low UTS values were estimated at around 209,

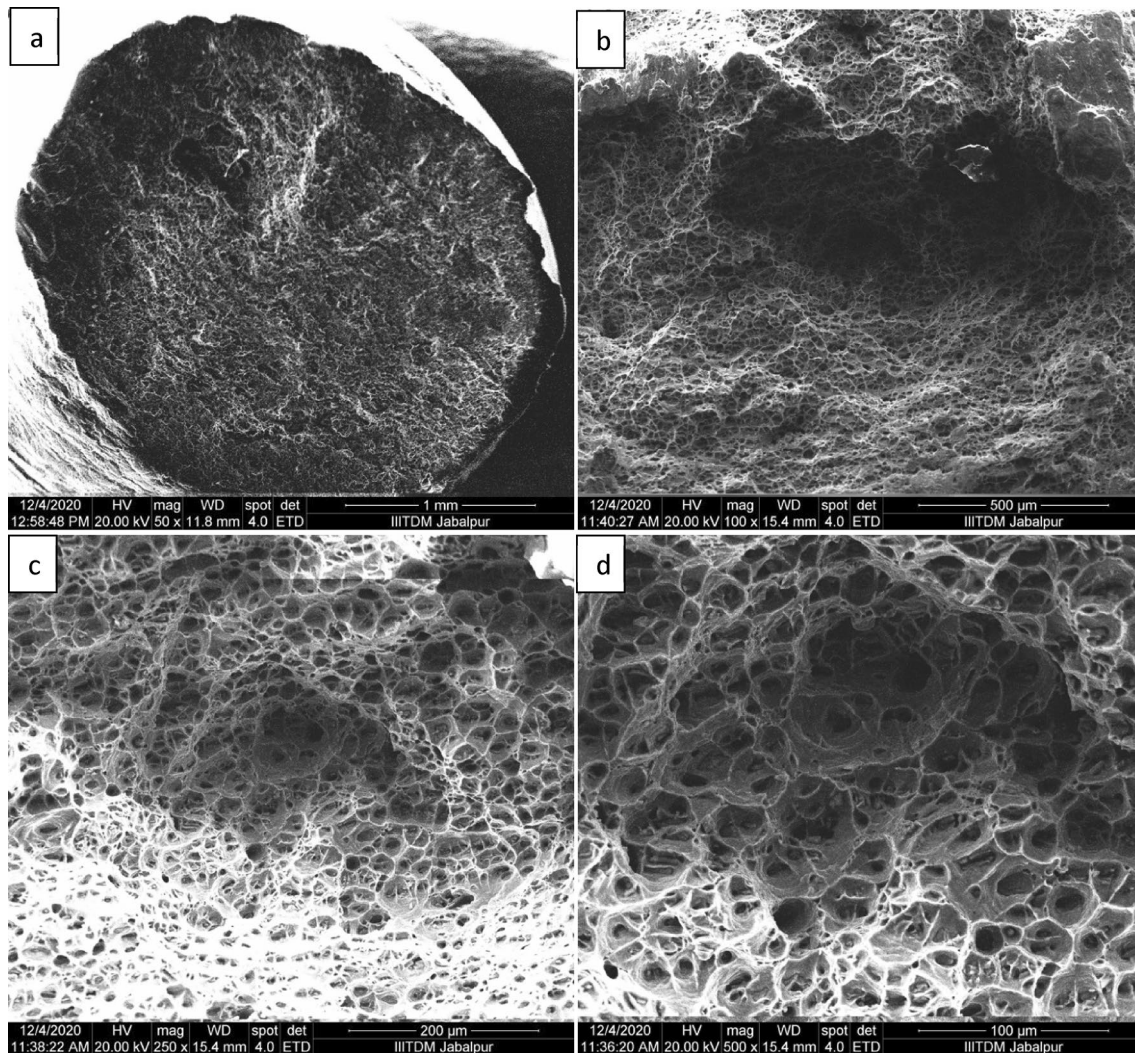


Fig. 10 a–d Fractography images of sample no. 12 (RS) at different magnifications

215, 211 and 210 MPa for experimental runs 7, 13, 17 and 25, respectively. Cause of their brittle failure and low UTS values has previously been explained.

On the other hand, larger and deeper dimples indicate greater energy involvement prior to failure. Fractography images of run numbers 23 and 24, as shown in Fig. 8a, b, respectively, exhibit higher UTS values of approximately 224 MPa, and display fine, densely populated, and deep dimples representing ductile fracture. Fractography images at AS and RS sample number 12 are presented as Figs. 9 and 10, respectively. Figure 9a represents fractography image AS at lower magnification while Fig. 9b–d represents fractography images at higher magnifications. It is evident from the images (Fig. 9) that dense deep and shallow dimples are present which indicates dimple fracture. Figure 10a–d illustrates fractography images of sample number 12 (RS).

Figure 10 also depicts dense and deep dimples which signify ductile fracture which corroborates the tensile results.

Conclusion

Following inferences can be drawn based on experimental investigation findings carried out throughout this work:

1. FSW is an effective method for welding thick AA6061-T6 alloys and results in high-quality joints.
2. Three process parameters, namely RST, TST, and SDT, were identified as variables.
3. The impact of these three variables on UTS as well as percentage elongation for welded joints was examined.

4. Influence of selected process parameters and their interactions upon UTS was investigated. The results indicated that the chosen parameters, as well as their interactions, have a significant effect on UTS. The optimal combination of process parameters for achieving maximum UTS was found to be A1B3C1 within the selected range.
5. The study revealed that TST had the most significant impact on UTS, contributing 25.94%, followed by SDT with 25.86% and RST with 20.30%. Additionally, the interactions between the selected parameters were found to be significant, with TSTSDT contributing 14.10%, followed by RSTTST with 6.51% and RST*SDT with 3.10%.
6. Chosen process parameters and their interactions in the specified ranges had a significant effect on percentage elongation, and the optimal combination of process parameters for achieving maximum percentage elongation was found to be A2B2C1.
7. The results showed that RST was the most significant process parameter affecting percentage elongation, with a contribution of 55.41%, followed by TST with 18.4% and SDT with 5.47%. The interactions between the selected parameters were also found to be significant, with RSTTST contributing 11.88%, followed by TST-SDT with 4.99% and RST*SDT with 0.90%.
8. The majority of the welds exhibited a bell-shaped bead, with top surfaces being approximately equal to SDT and the bottom bead surfaces being roughly equivalent to the diameter of the tool's pin.

Funding No funding.

Declarations

Conflict of interest The authors declare that they have no known competing financial interests or personal relationships that could have appeared to influence the work reported in this paper.

References

1. Z.Y. Ma, A.H. Feng, D.L. Chen, J. Shen, Recent advances in friction stir welding/processing of aluminum alloys: microstructural evolution and mechanical properties. *Crit. Rev. Solid State Mater. Sci.* **43**(4), 269–333 (2018)
2. G. Çam, G. İpekoğlu, Recent developments in joining of aluminum alloys. *Int. J. Adv. Manuf. Technol.* **91**(5), 1851–1866 (2017)
3. N. Khan, S. Rathee, M. Srivastava, Friction stir welding: an overview on effect of tool variables. *Mater. Today Proc.* **47**, 7196–7202 (2021)
4. A. Sharma et al., Friction stir lap welding of AA6061 aluminium alloy with a graphene interlayer. *Mater. Manuf. Process.* **35**(3), 258–269 (2020)
5. W.M. Thomas, E.D. Nicholas, J.C. Needham, M.G. Nurch, P. Temple-Smith, C. Dawes, Friction stir butt welding. *G.B.* (1991)
6. S. Rathee, S. Maheshwari, A. Noor Siddiquee, M. Srivastava, A review of recent progress in solid state fabrication of composites and functionally graded systems via friction stir processing. *Crit. Rev. Solid State Mater. Sci.* **43**(4), 334–366 (2018)
7. S. Rathee, S. Maheshwari, A. Noor Siddiquee, Issues and strategies in composite fabrication via friction stir processing: a review. *Mater. Manuf. Process.* **33**(3), 239–261 (2018)
8. A. Sharma, H. Fujii, J. Paul, Influence of reinforcement incorporation approach on mechanical and tribological properties of AA6061- CNT nanocomposite fabricated via FSP. *J. Manuf. Process.* **59**, 604–620 (2020)
9. A. Sharma, T. Das, J. Paul, Performance evaluation of Al6061-graphene nanocomposites surface engineered by a novel multiple microchannel reinforcement approach in friction stir processing. *Carbon Lett.* **31**(6), 1111–1124 (2021)
10. S. Rathee, S. Maheshwari, A. Noor Siddiquee, M. Srivastava, Distribution of reinforcement particles in surface composite fabrication via friction stir processing: suitable strategy. *Mater. Manuf. Process.* **33**(3), 262–269 (2018)
11. G.K. Padhy, C.S. Wu, S. Gao, Friction stir based welding and processing technologies: processes, parameters, microstructures and applications: a review. *J. Mater. Sci. Technol.* **34**(1), 1–38 (2018)
12. S. Rathee, M. Srivastava, S. Maheshwari, T.K. Kundra, A.N. Siddiquee, *Friction Based Additive Manufacturing Technologies: Principles for Building in Solid State, Benefits, Limitations, and Applications*, Ist. (CRC Press, Taylor & Francis, Boca Raton, 2018)
13. M. Srivastava, S. Rathee, S. Maheshwari, A.N. Siddiquee, T.K. Kundra, A review on recent progress in solid state friction based metal additive manufacturing: friction stir additive techniques. *Crit. Rev. Solid State Mater. Sci.* **44**(5), 345–377 (2019)
14. M. Srivastava, S. Rathee, S. Maheshwari, T.K. Kundra, *Additive Manufacturing: Fundamentals and Advancements* (CRC Press, Boca Raton, 2019)
15. S. Rathee, M. Srivastava, P.M. Pandey, A. Mahawar, S. Shukla, Metal additive manufacturing using friction stir engineering: a review on microstructural evolution, tooling and design strategies. *CIRP J. Manuf. Sci. Technol.* **35**, 560–588 (2021)
16. O.S. Salih et al., A review of friction stir welding of aluminium matrix composites. *Mater. Des.* **86**, 61–71 (2015)
17. R. Rai et al., Review: friction stir welding tools. *Sci. Technol. Weld. Joining* **16**(4), 325–342 (2011)
18. R. Palanivel, P. Koshy Mathews, N. Murugan, I. Dinaharan, Effect of tool rotational speed and pin profile on microstructure and tensile strength of dissimilar friction stir welded AA5083-H111 and AA6351-T6 aluminum alloys. *Mater. Des.* **40**, 7–16 (2012)
19. M. Srivastava, S. Rathee, A study on the effect of incorporation of SiC particles during friction stir welding of Al 5059 alloy. *SILICON* **13**(7), 2209–2219 (2021)
20. N. Khan, S. Rathee, M. Srivastava, C. Sharma, Effect of tool rotational speed on weld quality of friction stir welded AA6061 alloys. *Mater. Today Proc.* **47**, 7203–7207 (2021)
21. G. Çam, S. Mistikoglu, Recent developments in friction stir welding of Al-alloys. *J. Mater. Eng. Perform.* **23**(6), 1936–1953 (2014)
22. H.J. Liu, J.C. Hou, H. Guo, Effect of welding speed on microstructure and mechanical properties of self-reacting friction stir welded 6061-T6 aluminum alloy. *Mater. Des.* **50**, 872–878 (2013)

23. S. Malopheyev, I. Vysotskiy, V. Kulitskiy, S. Mironov, R. Kaibyshev, Optimization of processing-microstructure-properties relationship in friction-stir welded 6061–T6 aluminum alloy. *Mater. Sci. Eng. A* **662**, 136–143 (2016)
24. Software, M.S., Computer Software; Minitab State College, PA: Minitab, Inc. www.minitab.com. 2010

Springer Nature or its licensor (e.g. a society or other partner) holds exclusive rights to this article under a publishing agreement with the author(s) or other rightsholder(s); author self-archiving of the accepted manuscript version of this article is solely governed by the terms of such publishing agreement and applicable law.

Publisher's Note Springer Nature remains neutral with regard to jurisdictional claims in published maps and institutional affiliations.